Supplementary material to: "Theory of spin-orbit induced spin relaxation in functionalized graphene"

Jan Bundesmann, Denis Kochan, Fedor Tkatschenko, Jaroslav Fabian, and Klaus Richter
Institut für Theoretische Physik, Universität Regensburg, 93040 Regensburg, Germany

Adatom Hamiltonians

In the manuscript we use adatom Hamiltonians derived from symmetry and with parameters fitted to first-principles calculations, obtained for hydrogenated [1] and fluorinated [2] graphene. The full Hamiltonian $\mathcal{H}$ can be separated into the orbital $\mathcal{H}_{\rm orb}$ and SOC $\mathcal{H}_{\rm soc}$ parts. Introducing (spin-resolved) state $|d_{(\sigma)}\rangle$ for the adatom level and $|m_{(\sigma)}\rangle$ for the carbon $2p_z$-orbital at lattice site m [spin index $\sigma \in \{1,-1\} \equiv \{\uparrow,\downarrow\}$], we can write

$$\mathcal{H}_{\rm orb} = \mathcal{H}_{\rm gr} + \varepsilon \sum_{\sigma} |d_\sigma\rangle\langle d_\sigma| + \omega \sum_{\sigma} |d_\sigma\rangle\langle 0_\sigma| + \text{h.c.} \tag{1}$$

Here $\mathcal{H}_{\rm gr} = -t\sum_{\langle m,n\rangle,\sigma} |m_\sigma\rangle\langle n_\sigma|$ is the graphene nearest-neighbor hopping Hamiltonian ($t = 2.6$ eV), ε is the on-site energy of the adatom level and ω is the hopping integral between the adatom and its neighbor carbon.

Since the weak SOC of the pristine graphene does not play any significant role for the high adatom densities we consider, we focus only on the locally induced SOC effects in the vicinity of adatoms. The defect region consists of the adatomized carbon ($m = 0$) and sets $\mathrm{C_{nn}}$ and $\mathrm{C_{nnn}}$ of its three nearest (nn) and six next-nearest (nnn) neighbors. A realistic effective SOC Hamiltonian based on local symmetries was derived in Refs. [1, 2], and is given as follows:

$$\begin{aligned}
\mathcal{H}_{\rm soc} =& \frac{\mathrm{i}\Lambda_{\rm I}^{\rm A}}{3\sqrt{3}} \sum_{m\in \mathrm{C_{nnn}}} \sum_{\sigma} |0_\sigma\rangle\, \nu_{0m}\, (\hat{s}_z)_{\sigma\sigma}\, \langle m_\sigma| + \text{h.c.} \\
&+ \frac{\mathrm{i}\Lambda_{\rm I}^{\rm B}}{3\sqrt{3}} \sum_{\substack{m,n\in \mathrm{C_{nn}} \\ m\neq n}} \sum_{\sigma} |m_\sigma\rangle\, \nu_{mn}\, (\hat{s}_z)_{\sigma\sigma}\, \langle n_\sigma| \\
&+ \frac{2\mathrm{i}\Lambda_{\rm R}}{3} \sum_{m\in \mathrm{C_{nn}}} \sum_{\sigma\neq\sigma'} |0_\sigma\rangle\, (\hat{\boldsymbol{s}} \times \boldsymbol{d}_{0m})_{z,\sigma\sigma'}\, \langle m_{\sigma'}| + \text{h.c.} \\
&+ \frac{2\mathrm{i}\Lambda_{\rm PIA}^{\rm A}}{3} \sum_{m\in \mathrm{C_{nnn}}} \sum_{\sigma\neq\sigma'} |0_\sigma\rangle\, (\boldsymbol{d}_{0m} \times \hat{\boldsymbol{s}})_{z,\sigma\sigma'}\, \langle m_{\sigma'}| + \text{h.c.} \\
&+ \frac{2\mathrm{i}\Lambda_{\rm PIA}^{\rm B}}{3} \sum_{\substack{m,n\in \mathrm{C_{nn}} \\ m\neq n}} \sum_{\sigma\neq\sigma'} |m_\sigma\rangle\, (\boldsymbol{d}_{mn} \times \hat{\boldsymbol{s}})_{z,\sigma\sigma'}\, \langle n_{\sigma'}|\,.
\end{aligned} \tag{2}$$

Symbol $\hat{s}$ represents an array of the Pauli matrices acting in spin space. The sign factor ν_{mn} equals -1 $(+1)$ if the next-nearest hopping $n \to l \to m$ via a common neighbor l becomes (counter)clockwise and a unit vector $\boldsymbol{d}_{mn} = \frac{\mathbf{R}_m - \mathbf{R}_n}{|\mathbf{R}_m - \mathbf{R}_n|}$ points from site n to m. The first two terms in Eq. (2) are the local intrinsic SOCs associated with sublattices A and B, respectively, the third is the local Rashba SOC, and the last two terms are the local pseudospin inversion asymmetry (PIA) induced SOC for sublattices A and B, respectively; for more details see Refs. [1, 2]. The graphical representation of the orbital and local SOC hoppings is in Fig. **??**(a) and (b) of the manuscript, respectively. The numerical values of these parameters for hydrogenated and fluorinated graphene are summarized in Table I. We adopt these values for our numerical and analytical calculations of the spin relaxation rates.

Adatom	ω	ε	$\Lambda_{\rm I}^{\rm A}$	$\Lambda_{\rm I}^{\rm B}$	$\Lambda_{\rm R}$	$\Lambda_{\rm PIA}^{\rm A}$	$\Lambda_{\rm PIA}^{\rm B}$
Hydrogen	7.5	0.16	-0.21	0	0.33	0	0.77
Fluorine	5.5	-2.2	0	3.3	11.2	0	7.3

TABLE I. Orbital (in eV) and spin-orbital (in meV) tight-binding parameters entering the model Hamiltonians $\mathcal{H}_{\rm orb}$, Eq. (1), and $\mathcal{H}_{\rm soc}$, Eq. (2), for the dilute hydrogenated and fluorinated graphene structures, respectively, obtained from Ref. [1, 2].

Landauer transport simulation

Our numerical approach employs tight binding Hamiltonian $\mathcal{H} = \mathcal{H}_{\rm orb} + \mathcal{H}_{\rm soc}$ that consists of Eqs. (1) and (2). Properties of the infinitely extended graphene are approximated by specific periodic boundary conditions (PBC) that are applied to a finite scattering region [3**?**]. This means that we introduce additional hoppings connecting atomic sites on the opposite edges of the finite sample and, moreover, modify them by a complex phase factor $\exp(\mathrm{i}\Phi_B)$ in accordance with the Bloch theorem. For example, to study transport properties of a finite nanoribbon with SOC-active adatom and two attached parallel leads, we introduce PBC with a single phase Φ_B along the transverse direction. Alternatively, to calculate DOS, we employ PBC along the both longitudinal (x) and transverse (y) directions what requires two distinct Bloch phases Φ_x and Φ_y. Retarded Green's function G^r corresponding to $\mathcal{H}$ with specific PBC [Φ_B or (Φ_x, Φ_y)], is calculated by the recursive Green's function algorithm. From G^r we then obtain local (spin-)density of states [L(S)DOS] and scattering amplitudes within the framework of the Landauer-Büttiker formalism. However, the final results require averaging over the different PBC phases $\Phi_B, \Phi_x, \Phi_y \in [0, 2\pi[$. This is equivalent to averaging over the different transverse momenta and hence in fact over the different incoming and outgoing angles. The results of this Landauer-type calculation are the spin-flip probabilities of the reflected and transmitted electrons, over the defect region, as described in the manuscript.

T-matrix scattering formalism

Alternatively, we obtain spin relaxation rates analytically using the T-matrix formalism. We first integrate out the adatom $|d\rangle$-state and project the original Hamiltonian $\mathcal{H}_{\rm orb}$, Eq. (1) into an effective down-folded form

$$\mathcal{H}_{\rm orb}(E) = \mathcal{H}_{\rm gr} + \sum_{\sigma} \frac{\omega^2}{E-\varepsilon} \, |0_\sigma\rangle\langle 0_\sigma| \, . \tag{3}$$

The energy dependent on-site coupling $\omega^2/(E-\varepsilon)$ at the adatomized site $m = 0$, together with $\mathcal{H}_{\rm soc}$, Eq. (2), represent the interaction for our non-perturbative treatment. The interaction term $V = \sum_\sigma [\omega^2/(E-\varepsilon)] \, |0_\sigma\rangle\langle 0_\sigma| + \mathcal{H}_{\rm soc}$ is localized and couples only atomic sites m and n that are constrained to the vicinity of impurity, i.e., $V_{m,\sigma|n,\sigma'}$ is a finite matrix with $m, n \in \{0 \cup \mathrm{C_{nn}} \cup \mathrm{C_{nnn}}\}$; its entries are given in the following section for completeness. The same holds for the T-matrix, when expressed in the local atomic basis

$$\mathrm{T}_{m,\sigma|n,\sigma'}(E) = \big\langle m,\sigma \big| V \big[1 - G(E) V\big]^{-1} \big| n,\sigma' \big\rangle \, . \tag{4}$$

Since the matrix inversion can be readily performed, what is in fact needed are the unperturbed Green's function matrix elements $G_{m,\sigma|n,\sigma'}(E) = \langle m|1/(E_+ - \mathcal{H}_{\rm gr})|n\rangle \delta_{\sigma,\sigma'}$ for $m, n \in \{0 \cup \mathrm{C_{nn}} \cup \mathrm{C_{nnn}}\}$. Near the charge neutrality point $G_{m,\sigma|n,\sigma'}(E)$ can be computed analytically [4–6] (see also the next section), so $\mathrm{T}_{m,\sigma|n,\sigma'}(E)$ is known fully non-perturbatively.

Interaction Hamiltonian & Green's functions

The interaction Hamiltonian $V = \sum_\sigma [\omega^2/(E-\varepsilon)] \, |0_\sigma\rangle\langle 0_\sigma| + \mathcal{H}_{\rm soc}(\Lambda_{\rm I}^{\rm A}, \Lambda_{\rm I}^{\rm B}, \Lambda_{\rm R}, \Lambda_{\rm PIA}^{\rm B})$ can be in the local atomic basis $|m_\sigma\rangle$ expressed as $V_{m,\sigma|n,\sigma'} = M_{m,\sigma|n,\sigma'} + (M^\dagger)_{m,\sigma|n,\sigma'}$. Elements of the interaction matrix V, and hence of its reduced form M, are (potentially) non-zero only if $m, n \in \{0, \mathrm{b}_1, \mathrm{b}_2, \mathrm{b}_3, \mathrm{a}_1, \ldots, \mathrm{a}_6\} = \{0 \cup C_{\rm nn} \cup C_{\rm nnn}\}$. A graphical representation of our notation of the atomic positions near the adatom is shown in Fig. 1. Fixing the spin quantization axis along z-direction, the entries of M are summarized in Table II—for practical purposes we use there a reduced notation,

$$\tilde{\Lambda}_{\rm I}^{\rm A} = \tfrac{1}{3\sqrt{3}} \Lambda_{\rm I}^{\rm A} \, , \quad \tilde{\Lambda}_{\rm I}^{\rm B} = \tfrac{1}{3\sqrt{3}} \Lambda_{\rm I}^{\rm B} \, , \quad \tilde{\Lambda}_{\rm R} = \tfrac{2}{3} \Lambda_{\rm R} \, , \quad \tilde{\Lambda}_{\rm P}^{\rm B} = \tfrac{2}{3} \Lambda_{\rm PIA}^{\rm B} \, . \tag{5}$$

Ignoring spin degrees of freedom, the Bloch eigenstates $|\boldsymbol{\kappa}\rangle \equiv |\mathbf{q}, \tau, u\rangle$ of the unperturbed graphene problem $\mathcal{H}_{\rm gr} = -t \sum_{\langle m,n \rangle} |m\rangle\langle n|$ are in the low-energy limit labeled by the band index $u \equiv \mathrm{sgn}(E) = 1(-1)$ for the conduction (valence) band, the valley index $\tau = 1(-1)$ for the K (K′) point, and momentum $\mathbf{q}$ measured from the given valley. For a general lattice site m with a position vector $\mathbf{R}$ (non-necessarily a lattice vector) the amplitude of the low energy eigenstate $|\boldsymbol{\kappa}\rangle = |\mathbf{q}, \tau, u\rangle$ on that site is given as follows

$$\langle m|\boldsymbol{\kappa}\rangle = \frac{\chi_{\rm A}(m) + u\chi_{\rm B}(m)}{\sqrt{2}} \, e^{\mathrm{i}(\tau\mathbf{K}+\mathbf{q})\cdot\mathbf{R} - \mathrm{i}\tau\varphi_{\mathbf{q}}\chi_{\rm B}(m)} \, . \tag{6}$$

	$\langle 0_\uparrow\vert$	$\langle b_{1\uparrow}\vert$	$\langle b_{2\uparrow}\vert$	$\langle b_{3\uparrow}\vert$	$\langle a_{1\uparrow}\vert$	$\langle a_{2\uparrow}\vert$	$\langle a_{3\uparrow}\vert$	$\langle a_{4\uparrow}\vert$	$\langle a_{5\uparrow}\vert$	$\langle a_{6\uparrow}\vert$	$\langle 0_\downarrow\vert$	$\langle b_{1\downarrow}\vert$	$\langle b_{2\downarrow}\vert$	$\langle b_{3\downarrow}\vert$	$\langle a_{1\downarrow}\vert$	$\langle a_{2\downarrow}\vert$	$\langle a_{3\downarrow}\vert$	$\langle a_{4\downarrow}\vert$	$\langle a_{5\downarrow}\vert$	$\langle a_{6\downarrow}\vert$
$\vert 0_\uparrow\rangle$	$\frac{\omega^2}{2(E-\varepsilon)}$	0	0	0	$\mathrm{i}\tilde{\Lambda}_\mathrm{I}^\mathrm{A}$	$-\mathrm{i}\tilde{\Lambda}_\mathrm{I}^\mathrm{A}$	$\mathrm{i}\tilde{\Lambda}_\mathrm{I}^\mathrm{A}$	$-\mathrm{i}\tilde{\Lambda}_\mathrm{I}^\mathrm{A}$	$\mathrm{i}\tilde{\Lambda}_\mathrm{I}^\mathrm{A}$	$-\mathrm{i}\tilde{\Lambda}_\mathrm{I}^\mathrm{A}$	0	$\mathrm{i}\tilde{\Lambda}_\mathrm{R}$	$\mathrm{i}\tilde{\Lambda}_\mathrm{R}e^{\mathrm{i}\frac{4\pi}{3}}$	$\mathrm{i}\tilde{\Lambda}_\mathrm{R}e^{\mathrm{i}\frac{2\pi}{3}}$	0	0	0	0	0	0
$\vert b_{1\uparrow}\rangle$	0	0	$\mathrm{i}\tilde{\Lambda}_\mathrm{I}^\mathrm{B}$	$-\mathrm{i}\tilde{\Lambda}_\mathrm{I}^\mathrm{B}$	0	0	0	0	0	0	$-\mathrm{i}\tilde{\Lambda}_\mathrm{R}$	0	$\tilde{\Lambda}_\mathrm{P}^\mathrm{B}e^{\mathrm{i}\frac{2\pi}{3}}$	$-\tilde{\Lambda}_\mathrm{P}^\mathrm{B}e^{\mathrm{i}\frac{4\pi}{3}}$	0	0	0	0	0	0
$\vert b_{2\uparrow}\rangle$	0	0	0	$\mathrm{i}\tilde{\Lambda}_\mathrm{I}^\mathrm{B}$	0	0	0	0	0	0	$-\mathrm{i}\tilde{\Lambda}_\mathrm{R}e^{\mathrm{i}\frac{4\pi}{3}}$	$-\tilde{\Lambda}_\mathrm{P}^\mathrm{B}e^{\mathrm{i}\frac{2\pi}{3}}$	0	$\tilde{\Lambda}_\mathrm{P}^\mathrm{B}$	0	0	0	0	0	0
$\vert b_{3\uparrow}\rangle$	0	0	0	0	0	0	0	0	0	0	$-\mathrm{i}\tilde{\Lambda}_\mathrm{R}e^{\mathrm{i}\frac{2\pi}{3}}$	$\tilde{\Lambda}_\mathrm{P}^\mathrm{B}e^{\mathrm{i}\frac{4\pi}{3}}$	$-\tilde{\Lambda}_\mathrm{P}^\mathrm{B}$	0	0	0	0	0	0	0
$\vert a_{1\uparrow}\rangle$	0	0	0	0	0	0	0	0	0	0	0	0	0	0	0	0	0	0	0	0
$\vert a_{2\uparrow}\rangle$	0	0	0	0	0	0	0	0	0	0	0	0	0	0	0	0	0	0	0	0
$\vert a_{3\uparrow}\rangle$	0	0	0	0	0	0	0	0	0	0	0	0	0	0	0	0	0	0	0	0
$\vert a_{4\uparrow}\rangle$	0	0	0	0	0	0	0	0	0	0	0	0	0	0	0	0	0	0	0	0
$\vert a_{5\uparrow}\rangle$	0	0	0	0	0	0	0	0	0	0	0	0	0	0	0	0	0	0	0	0
$\vert a_{6\uparrow}\rangle$	0	0	0	0	0	0	0	0	0	0	0	0	0	0	0	0	0	0	0	0
$\vert 0_\downarrow\rangle$	0	0	0	0	0	0	0	0	0	0	$\frac{\omega^2}{2(E-\varepsilon)}$	0	0	0	$-\mathrm{i}\tilde{\Lambda}_\mathrm{I}^\mathrm{A}$	$\mathrm{i}\tilde{\Lambda}_\mathrm{I}^\mathrm{A}$	$-\mathrm{i}\tilde{\Lambda}_\mathrm{I}^\mathrm{A}$	$\mathrm{i}\tilde{\Lambda}_\mathrm{I}^\mathrm{A}$	$-\mathrm{i}\tilde{\Lambda}_\mathrm{I}^\mathrm{A}$	$\mathrm{i}\tilde{\Lambda}_\mathrm{I}^\mathrm{A}$
$\vert b_{1\downarrow}\rangle$	0	0	0	0	0	0	0	0	0	0	0	0	0	0	0	0	0	0	0	0
$\vert b_{2\downarrow}\rangle$	0	0	0	0	0	0	0	0	0	0	0	0	0	0	0	0	0	0	0	0
$\vert b_{3\downarrow}\rangle$	0	0	0	0	0	0	0	0	0	0	0	0	0	0	0	0	0	0	0	0
$\vert a_{1\downarrow}\rangle$	0	0	0	0	0	0	0	0	0	0	0	0	0	0	0	0	0	0	0	0
$\vert a_{2\downarrow}\rangle$	0	0	0	0	0	0	0	0	0	0	0	0	0	0	0	0	0	0	0	0
$\vert a_{3\downarrow}\rangle$	0	0	0	0	0	0	0	0	0	0	0	0	0	0	0	0	0	0	0	0
$\vert a_{4\downarrow}\rangle$	0	0	0	0	0	0	0	0	0	0	0	0	0	0	0	0	0	0	0	0
$\vert a_{5\downarrow}\rangle$	0	0	0	0	0	0	0	0	0	0	0	0	0	0	0	0	0	0	0	0
$\vert a_{6\downarrow}\rangle$	0	0	0	0	0	0	0	0	0	0	0	0	0	0	0	0	0	0	0	0

TABLE II. Matrix elements of the reduced interaction M. The full interaction V (orbital chemisorption plus SOC) then becomes $V = M + M^\dagger$. Rows and columns are labeled by local atomic (bra and ket) states $|m_\sigma\rangle$, where $m = \{0, \mathrm{b}_1, \mathrm{b}_2, \mathrm{b}_3, \mathrm{a}_1, \ldots, \mathrm{a}_6\}$; for the description of the atomic positions see Fig. 1.

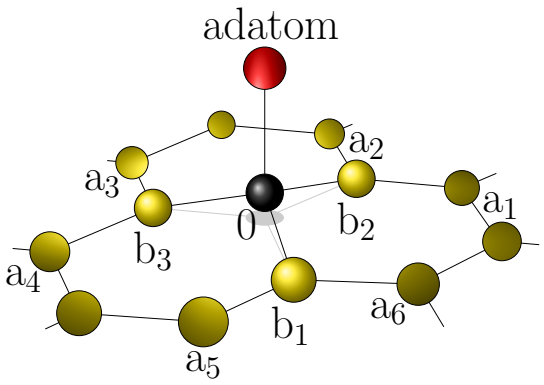

FIG. 1. Atomic positions of relevant carbon atoms in the vicinity of an adatom. Adatomized carbon is denoted as 0 ($m = 0$ site), its three nearest neighbors as $\mathrm{b}_1, \mathrm{b}_2, \mathrm{b}_3$, and the six next-nearest neighbors as $\mathrm{a}_1, \ldots, \mathrm{a}_6$.

Here $\chi_{\mathrm{A}}(m)$ equals one (zero) if the lattice site m belongs to the sublattice A (B) and vice versa for $\chi_{\mathrm{B}}(m)$, $\varphi_{\mathbf{q}}$ is the polar angle of vector $\mathbf{q}$ with respect to x-axis, and $\mathbf{K} = \frac{4\pi}{3}(1, 0)$ is the position of the K point in the reciprocal lattice ($a = \sqrt{3}a_{\mathrm{cc}} = 2.46\,\text{Å}$). The Bloch states $|\boldsymbol{\kappa}\rangle$ are normalized to graphene unit cell, i.e. $\langle\boldsymbol{\kappa}|\boldsymbol{\kappa}\rangle = \sum_m |\langle m|\boldsymbol{\kappa}\rangle|^2 = M$, where M is the number of unit cells within the sample. This is very practical since the T-matrix in the position-space couples only a finite number of atomic sites, hence computing $\mathrm{T}_{\boldsymbol{\kappa},\sigma|\boldsymbol{\kappa}',\sigma'} = \langle\boldsymbol{\kappa},\sigma|\mathrm{T}|\boldsymbol{\kappa}',\sigma'\rangle$ reduces to a finite matrix multiplication

$$\mathrm{T}_{\boldsymbol{\kappa},\sigma|\boldsymbol{\kappa}',\sigma'} = \sum_{m,n} \langle\boldsymbol{\kappa}|m\rangle\, \mathrm{T}_{m,\sigma|n,\sigma'}\, \langle n|\boldsymbol{\kappa}'\rangle\,, \qquad \text{where} \quad m, n \in \{0 \cup \mathrm{C_{nn}} \cup \mathrm{C_{nnn}}\}\,. \tag{7}$$

In the range of energies for which the graphene linear dispersion applies,

$$\epsilon(\tau\mathbf{K} + \mathbf{q}) = \pm\frac{3}{2}a_{\mathrm{cc}}t|\mathbf{q}| = \pm\hbar v_{\mathrm{F}}|\mathbf{q}| \tag{8}$$

($a_{\mathrm{cc}} = 1.42\,\text{Å}$, $t = 2.6\,\mathrm{eV}$, and $\hbar v_{\mathrm{F}} \simeq 5.5\ \mathrm{eV\,Å}$), the retarded Green's function elements in real space can be computed analytically [4–6]. For a geometry in which the x-axis is parallel with the graphene zig-zag edge, and y-axis is aligned with the graphene armchair direction, see Fig. 1, the result is as follows

$$G_{m|m}(E) = \frac{E}{W^2}\ln\frac{E^2}{W^2 - E^2} - i\pi\frac{|E|}{W^2}\,, \tag{9}$$

$$G_{m|n}(E) = \frac{\pi}{\mathrm{i}}\frac{|E|}{W^2}H_0^{(\frac{3-u}{2})}\left(\tfrac{|E|}{\hbar v_{\mathrm{F}}}|\mathbf{R}|\right)\cos\mathbf{K}\cdot\mathbf{R}\,, \tag{10}$$

$$G^{\mathrm{A,B}}_{m|n}(E) = \mathrm{i}\pi\frac{E}{W^2}H_1^{(\frac{3-u}{2})}\left(\tfrac{|E|}{\hbar v_{\mathrm{F}}}|\mathbf{R}|\right)\sin[\mathbf{K}\cdot\mathbf{R} + \theta_{\mathbf{R}}]\,. \tag{11}$$

Here $u \equiv \mathrm{sgn}(E)$ should be properly applied to guarantee the retardness of $G(E)$. Equation (9) gives the on-site retarded Green's function, where $W = \sqrt{\sqrt{3}\pi}t \simeq 6$ eV is the effective graphene bandwidth and

$$-\frac{1}{\pi}\mathrm{Im}\,G_{m|m}(E) \equiv \nu_0(E) = \frac{|E|}{W^2} \tag{12}$$

is the associated DOS per atom and spin (in the low energy limit, well applicable within the energy window $[-1; 1]$ eV). For two different atomic sites $m \neq n$ on the same and opposite sublattices we have correspondingly Eqs. (10) and (11). There $\mathbf{K} = \frac{4\pi}{3a}(1, 0)$ stands for the K-point, $\mathbf{R} = m - n$ is the vector pointing from the atomic site n to m and $0 \leq \theta_{\mathbf{R}} \leq \pi$ is the polar angle of $\mathbf{R}$ with respect to x-axis. To stress that $m \in$ A and $n \in$ B belong to opposite sublattices we have explicitly written in Eq. (11) the superscripts A and B, while symbols without the superscripts are reserved for the sites on the same sublattice. Complementary, $G^{\mathrm{B,A}}_{m|n}(E) = G^{\mathrm{A,B}}_{n|m}(E)$ and the Hankel's functions of the first $H^{(1)}(x)$ and second kind $H^{(2)}(x)$ are defined conventionally as $H^{(1)}(x) = J(x) + iY(x) = \overline{H^{(2)}}(x)$.

To analyze scattering we need asymptotic properties of $G(E)$ for $|\mathbf{R}| = |m - n| \gg 0$ (assuming the interaction V is supported around the origin of the coordinate system). Using the asymptotic expansions for the Hankel functions

$$H^{(1)}_{\alpha}(x) \simeq \sqrt{\frac{2}{\pi x}}\, e^{\mathrm{i}[x - \frac{\pi}{4}(2\alpha+1)]} \simeq \overline{H^{(2)}_{\alpha}}(x) \tag{13}$$

(in our case $\alpha = 0, 1$) we can write:

$$G_{m|n}(E) \simeq -ue^{+\mathrm{i}u\frac{\pi}{4}} \sqrt{\frac{2\pi\hbar v_F|E|}{W^4}} \frac{1}{\sqrt{|\mathbf{R}|}} e^{\mathrm{i}u\left(\frac{|E|}{\hbar v_\mathrm{F}}|\mathbf{R}|\right)} \cos \mathbf{K}\cdot\mathbf{R}\,, \tag{14}$$

$$G^{\mathrm{A,B}}_{m|n}(E) \simeq -ue^{-\mathrm{i}u\frac{\pi}{4}} \sqrt{\frac{2\pi\hbar v_F|E|}{W^4}} \frac{1}{\sqrt{|\mathbf{R}|}} e^{\mathrm{i}u\left(\frac{|E|}{\hbar v_\mathrm{F}}|\mathbf{R}|\right)} \sin[\mathbf{K}\cdot\mathbf{R} + \theta_{\mathbf{R}}]\,. \tag{15}$$

We see that apart from phase prefactors (important for Lippmann-Schwinger scattering solutions) the Green's function for $|\mathbf{R}| = |m-n| \gg 0$ has a form of a modulated circular wave with momentum $|\mathbf{q}| = |E|/(\hbar v_\mathrm{F})$. For $u = \operatorname{sgn} E = 1$ (electrons) it is a center-outgoing circular wave, while for $u = \operatorname{sgn} E = -1$ (holes) it is a center-incoming circular wave (electron moving toward a center = hole moving outward of a center).

Destructive interference between the Rashba and PIA spin-orbit couplings in fluorinated graphene

The PIA SOC, $\Lambda^{\mathrm{B}}_{\mathrm{PIA}}$, connects the nearest neighbor $\mathrm{C_{nn}}$ sites denoted at Fig. 1 as $\{\mathrm{b}_1, \mathrm{b}_2, \mathrm{b}_3\}$. Let us look how the $\Lambda^{\mathrm{B}}_{\mathrm{PIA}}$ interaction "renormalizes" in the presence of the local Rashba term, Λ_R, that couples $\mathrm{C_{nn}}$ sites with the central adatomized carbon 0, see Fig. 1(b) in the main section or Eq. (2). For concreteness we focus on a spin-down to spin-up hopping between the b_2 and b_3 sites, respectively. In the first order of SOC strengths there are three competing processes that could interfere. The first is PIA mediated direct spin-flip hopping $|\mathrm{b}_2,\downarrow\rangle \xrightarrow{\mathrm{PIA}} |\mathrm{b}_3,\uparrow\rangle$. The second and third combine orbital (spin-conserving t mediated) and Rashba (spin-flip Λ_R mediated) hoppings on/off the central site 0, i.e. $|\mathrm{b}_2,\downarrow\rangle \xrightarrow{\mathrm{R}} |0,\uparrow\rangle \xrightarrow{t} |\mathrm{b}_3,\uparrow\rangle$ and $|\mathrm{b}_2,\downarrow\rangle \xrightarrow{t} |0,\downarrow\rangle \xrightarrow{\mathrm{R}} |\mathrm{b}_3,\uparrow\rangle$. All these processes are governed by the part of the full Hamiltonian $\mathcal{H}_\mathrm{orb} + V$ given as follows, see Table II and Eqs. (5):

	$\langle \mathrm{b}_{2\uparrow}\vert$	$\langle \mathrm{b}_{3\downarrow}\vert$	$\langle 0_\uparrow\vert$	$\langle 0_\downarrow\vert$
$\vert \mathrm{b}_{2\uparrow}\rangle$	0	$\frac{2}{3}\Lambda^{\mathrm{B}}_{\mathrm{PIA}}$	$-t$	$-\mathrm{i}\frac{2}{3}\Lambda_\mathrm{R} e^{\mathrm{i}\frac{4\pi}{3}}$
$\vert \mathrm{b}_{3\downarrow}\rangle$	$\frac{2}{3}\Lambda^{\mathrm{B}}_{\mathrm{PIA}}$	0	$-\mathrm{i}\frac{2}{3}\Lambda_\mathrm{R} e^{\mathrm{i}\frac{4\pi}{3}}$	$-t$
$\vert 0_\uparrow\rangle$	$-t$	$\mathrm{i}\frac{2}{3}\Lambda_\mathrm{R} e^{\mathrm{i}\frac{2\pi}{3}}$	$\frac{\omega^2}{E-\varepsilon}$	0
$\vert 0_\downarrow\rangle$	$\mathrm{i}\frac{2}{3}\Lambda_\mathrm{R} e^{\mathrm{i}\frac{2\pi}{3}}$	$-t$	0	$\frac{\omega^2}{E-\varepsilon}$

(16)

In the case of fluorine, the on-site energy $\varepsilon = -2.2\,\mathrm{eV}$ is much larger then experimentally accessible energies E and hence we can approximate the effective on-site potential $\omega^2/(E-\varepsilon)$ in the above matrix by $-\omega^2/\varepsilon \simeq 13.8\,\mathrm{eV}$. To grasp the interference among three discussed paths we get rid off the intermediate $|0_\uparrow\rangle$ and $|0_\downarrow\rangle$ states by means of the Löwdin transformation arriving at the effective Hamiltonian in $|\mathrm{b}_{2\uparrow}\rangle$—$|\mathrm{b}_{3\downarrow}\rangle$ sector:

	$\langle \mathrm{b}_{2\uparrow}\vert$	$\langle \mathrm{b}_{3\downarrow}\vert$
$\vert \mathrm{b}_{2\uparrow}\rangle$	$-t_\mathrm{eff}$	$\frac{2}{3}\Lambda^{\mathrm{PIA}}_\mathrm{eff}$
$\vert \mathrm{b}_{3\downarrow}\rangle$	$\frac{2}{3}\Lambda^{\mathrm{PIA}}_\mathrm{eff}$	$-t_\mathrm{eff}$

where

$$t_\mathrm{eff} = -\left(t^2 + \frac{4}{9}\Lambda^2_\mathrm{R}\right)\frac{\varepsilon}{\omega^2} \simeq 0.5\,\mathrm{eV}\,,$$
$$\Lambda^{\mathrm{PIA}}_\mathrm{eff} = \Lambda^{\mathrm{B}}_{\mathrm{PIA}} + \sqrt{3}t\Lambda_\mathrm{R}\frac{\varepsilon}{\omega^2} \simeq 3.6\,\mathrm{meV}\,. \tag{17}$$

The on-site energy ε on the fluorine adatom is negative and hence the "renormalized" PIA SOC, $\Lambda^{\mathrm{PIA}}_\mathrm{eff}$, is by cca 50% smaller then the original $\Lambda^{\mathrm{B}}_{\mathrm{PIA}} = 7.3\,\mathrm{meV}$ coupling. Effectively we also get the next-nearest neighbor interaction mediated by t_eff, but since $t_\mathrm{eff} \ll t = 2.6\,\mathrm{eV}$ we can ignore this term on the orbital energy scale. So we showed that in the fluorinated graphene the Rashba and PIA mediated SOC interactions interfere destructively and, moreover, instead of

$$\mathcal{H}^{\mathrm{R}}_\mathrm{soc} + \mathcal{H}^{\mathrm{PIA}}_\mathrm{soc} = \frac{2\mathrm{i}\Lambda_\mathrm{R}}{3} \sum_{m\in\mathrm{C_{nn}}} \sum_{\sigma\neq\sigma'} |0_\sigma\rangle \left(\hat{\boldsymbol{s}}\times\boldsymbol{d}_{0m}\right)_{z,\sigma\sigma'} \langle m_{\sigma'}| + \frac{2\mathrm{i}\Lambda^{\mathrm{B}}_{\mathrm{PIA}}}{3} \sum_{\substack{m,n\in\mathrm{C_{nn}}\\ m\neq n}} \sum_{\sigma\neq\sigma'} |m_\sigma\rangle \left(\boldsymbol{d}_{mn}\times\hat{\boldsymbol{s}}\right)_{z,\sigma\sigma'} \langle n_{\sigma'}| + \mathrm{h.c.}\,, \tag{18}$$

one can employ the effective spin-flip Hamiltonian

$$\mathcal{H}^{\mathrm{PIA}}_\mathrm{eff} = \frac{2\mathrm{i}}{3}\Lambda^{\mathrm{PIA}}_\mathrm{eff} \sum_{\substack{m,n\in\mathrm{C_{nn}}\\ m\neq n}} \sum_{\sigma\neq\sigma'} |m_\sigma\rangle \left(\boldsymbol{d}_{mn}\times\hat{\boldsymbol{s}}\right)_{z,\sigma\sigma'} \langle n_{\sigma'}|\,. \tag{19}$$

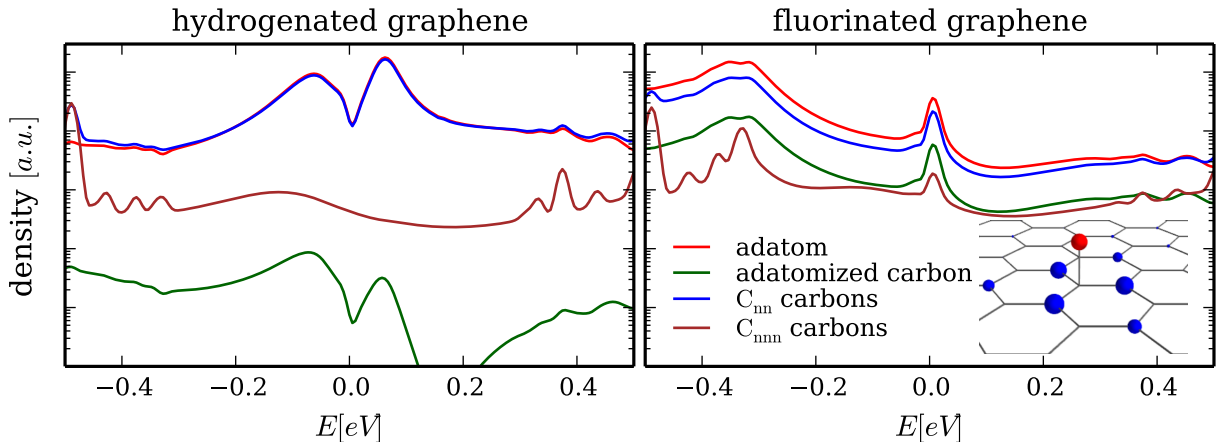

FIG. 2. (Color online) Calculated local density of states in the vicinity of hydrogen (left panel) and fluorine (right panel) adatom on graphene. The energy dependent LDOS's for the adatom (red), adatomized carbon (black), its three nearest neighbors C_{nn} (blue), and six next-nearest neighbors C_{nnn} (brown) are shown. In the case of hydrogenated graphene we see a strongly enhanced electron density at H and C_{nn} sites. At the same time LDOS drops significantly at the adatomized carbon for $E = \varepsilon = 0.16\,\mathrm{eV}$. For fluorinated graphene the differences in LDOS are much less dramatic.

Local density of states in the vicinity of adatoms

In the manuscript we argue that the reason for the reduced roles of the Rashba and intrinsic SOC terms in hydrogenated graphene is the vanishing local density of states (LDOS) at the adatomized carbon. Here we elaborate this issue further. From the on-site Green's function, such as Eq. (9), we can calculate the local density of states (LDOS), $\nu_m(E)$, at given site m using

$$\nu_m(E) = -\frac{1}{\pi}\mathrm{Im}\, G_{m|m}(E). \tag{20}$$

The relative population of various lattice sites enables us to understand the influence of the different types of local spin-orbit couplings. The relevant lattice sites that enter SOC Hamiltonian $\mathcal{H}_{\mathrm{soc}}$, Eq. (2) are plotted in Fig. 2 for hydrogenated and fluorinated graphene, respectively.

For hydrogenated graphene we find, for a very wide energy range, that the LDOS on the adatom is significantly larger than on the adatomized $m = 0$ carbon site directly chemisorbed with hydrogen. LDOS on its three nearest neighbors C_{nn} reaches values similar to those on the adatom. Increasing the distance to the adatom we observe again a decrease of the LDOS. Assuming the adatom sits on top of carbon in sublattice A, we find a suppression of the LDOS on the sublattice A with respect to sublattice B in the vicinity of hydrogen. The situation is similar in fluorinated graphene, but differences are much less pronounced in the given energy window shown at Fig. 2. This is because the on-site energy at fluorine $\varepsilon = -2.2\,\mathrm{eV}$—energy at which the LDOS redistribution between the sublattices is most important due to the $\omega^2/(E-\varepsilon)$ factor in the down-folded Hamiltonian—is far away from the resonance energy $E_{\mathrm{res}} \sim -260\,\mathrm{meV}$ at which the impurity region is populated by charge carriers.

In the manuscript we present the energy dependence of the spin-relaxation rates in hydrogenated and fluorinated graphene. For a qualitative explanation we need to consider also the LDOS on the involved atomic sites entering the SOC Hamiltonian since effectively, the spin-flipping/conserving probability is proportional to $|\Lambda|^2\nu(\mathrm{C}_1)\nu(\mathrm{C}_2)$, where $\nu(\mathrm{C}_i)$ stands for the LDOS at carbons C_1 and C_2 and Λ represents a SOC hopping connecting them. If the adatom is located on top of sublattice A the electron density on the opposite sublattice B is partially enhanced. Since in hydrogenated graphene within the relevant energy range the LDOS on sublattice A is several orders of magnitude smaller than on sublattice B, SOC terms which involve sublattice A—local intrinsic SOC $\Lambda_{\mathrm{I}}^{\mathrm{A}}$ and Rashba SOC Λ_{R}—should be less important than the PIA SOC term which is fully located on sublattice B. This is confirmed from our analytical and numerical-transport-based calculations. We find that it is only the PIA SOC which governs the spin-relaxation rate in hydrogenated graphene, see Fig. 2 in the manuscript. For getting the corresponding spin-relaxation rate $1/\tau_{s,\Lambda}$ we should multiply the probability $|\Lambda|^2\nu(\mathrm{C}_1)\nu(\mathrm{C}_2)$ with the graphene DOS which is proportional to energy

E. As a result we get the following energy scaling for the relaxation rates due to various SOC mechanisms:

$$1/\tau_{s,\mathrm{PIA}} \propto \tfrac{2\pi}{\hbar} E\,|\Lambda^{\mathrm{B}}_{\mathrm{PIA}}|^2\,\nu(\mathrm{C_B})\,\nu(\mathrm{C_B})\,, \tag{21}$$

$$1/\tau_{s,\mathrm{Rashba}} \propto \tfrac{2\pi}{\hbar} E\,|\Lambda_{\mathrm{R}}|^2\,\nu(\mathrm{C_0})\,\nu(\mathrm{C_B})\,, \tag{22}$$

$$1/\tau_{s,\mathrm{IntA}} \propto \tfrac{2\pi}{\hbar} E\,|\Lambda^{\mathrm{A}}_{\mathrm{I}}|^2\,\nu(\mathrm{C_0})\,\nu(\mathrm{C_A})\,. \tag{23}$$

Equations (21) - (23) can be used to qualitatively describe our spin-relaxation results in hydrogenated graphene.

For fluorine adatoms we find that there is no marked dependence of $\tau^{-1}_{s,\mathrm{IntB}}$ on the local densities of states. However, $\nu(\mathrm{C_B})$ drops at off-resonant energies and the influence of the intrinsic SOC should be somewhat enhanced. This enhancement is mainly visible in the anisotropy ratio between the out-of-plane and in-plane spin-relaxation rate, presented in the main text. For PIA and Rashba SOC this is ratio is 2, so in systems where one of these types of SOC dominate anisotropy should simply be two. A deviation can be expected if the intrinsic SOC prevails as this increases the in-plane spin-relaxation while keeping the out-of-plane relaxation untouched. This is precisely what happens in fluorinated graphene at positive energies, see the manuscript.

[1] M. Gmitra, D. Kochan, and J. Fabian, Phys. Rev. Lett. **110**, 246602 (2013).
[2] S. Irmer, T. Frank, S. Putz, M. Gmitra, D. Kochan, and J. Fabian, Phys. Rev. B **91**, 115141 (2015).
[3] M. Wimmer, *Quantum transport in nanostructures: From computational concepts to spintronics in graphene and magnetic tunnel junctions*, Ph.D. thesis, Universität Regensburg (2009).
[4] Z. F. Wang, R. Xiang, Q. W. Shi, J. Yang, X. Wang, J. G. Hou, and J. Chen, Phys. Rev. B **74**, 125417 (2006).
[5] M. Sherafati and S. Satpathy, Phys. Rev. B **83**, 165425 (2011).
[6] F. Ducastelle, Phys. Rev. B **88**, 075413 (2013).